

# Pulsatile flow of non-Newtonian fluid in stenosed micro channel

Eunseop Yeom,<sup>1\*</sup> Hyeonji Hong<sup>1</sup>, Jae Min Song<sup>2</sup>

<sup>1</sup> School of Mechanical Engineering, Pusan National University, Busan, South Korea

<sup>2</sup> School of Dentistry, Pusan National University, Busan, South Korea

E-mail: \*esyecom@pusan.ac.kr

## Abstract

For studying blood flow in the vessels, the non-Newtonian behavior of blood is important, considering the role of viscosity in rheology. An abnormal narrowing of the vessel called as stenosis has an influence on flow behavior. Therefore, flow measurement of blood flow in stenosed vessels is essential. However, most of studies exist as simulation outcomes. In this study, flow fields for non-Newtonian fluid were measured in stenosed microchannels under the pulsatile flow condition. A polydimethylsiloxane channel with 60% stenosis was fabricated by combining an optic fiber and a petri dish, resembling a mold. Non-Newtonian fluid were prepared by changing the concentrations of xanthan gum, which induces a shear thinning effect (two non-Newtonian fluids mimicking normal blood and highly viscous blood analog). The viscosity of the samples was measured using a Y-shaped microfluidic viscometer. Thereafter, velocity profiles were analyzed under the pulsatile flow condition using the micro-particle image velocimetry (PIV) method. The velocity profile of the non-Newtonian fluid was generally blunter compared to that of the Newtonian fluid. A highly oscillating wall shear stress (WSS) during the pulsatile phase may be attributed to such a bluntness of flow under the same wall shear rate condition with the Newtonian fluid. In addition, a highly viscous flow contributes to the variation in the WSS after passing through the stenosed structures. These results are well matched with the simulation results. Such a variation in the WSS was associated with plaque instability or rupture and damage of the tissue layer.

## 1 Introduction

The features of pulsatile blood flow in the vessels are complex and unsteady, so it is not easy to comprehend hemodynamic features completely (Jahangiri et al., 2018). For understanding blood flows in the vessels, Newtonian fluids, such as mixtures of glycerol and water models, have been widely used (Hong et al., 2017; Nguyen et al., 2004). Although the results using Newtonian fluids may be reasonable for large-scale channels mimicking arteries, the non-Newtonian behavior of the blood can change the viscosity at a low shear strain rate (Chien, 1970; Wells et al., 1961). In addition, blood viscosity influences flow resistance, and an increased viscosity is a biological parameter related to cardiovascular diseases (Torraldo et al., 2013). Therefore, flow analysis based on Newtonian fluid is insufficiently illustrate actual cardiovascular flow at low shear rate regions, such as downstream of stenosis in small-diameter vessels. By deposition of cholesterol and other relevant lipids, stenosis is formed, narrowing the blood vessels and affecting flow behavior (Molla et al., 2012). As the blood flows through stenosed channels, hemodynamic

characteristics, such as velocity vector, wall shear rate (WSR), and wall shear stress (WSS), calculated by multiplying blood viscosity and WSR are varied (Kwak et al., 2014). Many numerical studies have been conducted to analyze the distributions of velocity, WSS, and pressure around stenotic structures.

In this study, pulsatile flow of non-Newtonian fluid in a polydimethylsiloxane (PDMS) microchannel with stenosis was measured using the micro-particle image velocimetry (PIV). The velocity profiles and WSS were analyzed depending on the phase states and the positions in the microchannel. To measure the value of the WSS accurately, viscosity was also evaluated depending on the shear rates using a Y-shaped microfluidic viscometer (Yeom et al., 2017).

## **2 Materials and methods**

### **2.1. Fabrication of PDMS microchannel**

To stimulate stenosis geometry in the microchannel, PDMS microchannel was fabricated using a polymethylmethacrylate optic fiber with a diameter of 500  $\mu\text{m}$  (Mannino et al., 2015). The optic fiber in the middle part was sanded using a sharp edge of a sandpaper until its degree of stenosis reached 60% with the stenosis length of 1260  $\mu\text{m}$ . After fixing the optic fiber in the center of a petri dish, PDMS (Sylgard 184, Dow Corning, USA) was then poured into the mold. It was completely cured at 85°C and then removed from the petri dish. And then, the optic fiber was pulled out from the PDMS channel. By selecting the 60% severity of stenosis, the microchannel reflected the moderate stenosis state, which may progress depending on environmental influences.

### **2.2. Experimental setup**

PDMS stenosed channel was mounted on an optical microscope (IX2, Olympus, Tokyo, Japan) with an objective lens at 10 $\times$  magnification (NA of 0.1). It was illuminated by a 100-W halogen lamp. Flows in the microfluidic device were consecutively captured using a high-speed camera (Phantom VEO710L, Vision Research Inc., NJ, USA) at 400 frames per second (fps). Samples were supplied into the microchannel using a programmable syringe pump (neMESYS, Centoni GmbH, Germany) with a 1-mL plastic syringe (BD; Becton Dickinson, NJ, USA). All experiments were conducted at 25°C.

### **2.3. Working fluids**

For the non-Newtonian fluid, two types of samples were prepared by mixing water, glycerol, and xanthan gum. Two non-Newtonian samples with different concentrations of xanthan gum, which is a polysaccharide, were created. Since xanthan gum has a shear thinning characteristic, the viscosity of xanthan gum solutions decreases with increased shear rates. Sample 1 consisted of 79.1% (v/v) distilled water, 20.9% (v/v) glycerol, and 0.21 g/L of xanthan gum for a blood analog fluid (Anastasiou et al., 2012). Sample 2 comprised 0.42 g/L of xanthan gum under the same volumetric ratio of water and glycerol. Sample 2 has a two-fold higher concentration of xanthan gum than Sample 1 for observing the effect on flow characteristics under highly viscous blood.

### **2.4. Micro-PIV**

For obtaining velocity information using the micro-PIV method, tracer particles were added in the sample fluids with 0.2% solid proportion. The particles were polymer microspheres with a 0.52- $\mu\text{m}$  diameter (Fluoro-Max, Thermo SCIENTIFIC, USA). The center plane of 3-dimensional microchannel was focused

with the appropriate depth by the optics of the imaging system. In the present setup, depth of correlation expressing the depth over which particles contribute to the cross-correlation analysis is about 20  $\mu\text{m}$  (Yeom et al., 2014). After capturing images using a high-speed camera at 400 fps, they underwent post-processing, including cropping and masking. The sequence images were converted into velocity vector fields using a commercial program (PIVview2C, PIVTEC GmbH, Germany). The size of the interrogation window was  $32 \times 8$  pixels with 50% overlapping. MATLAB software (Mathworks, USA) was utilized for analyzing velocity data.

## 2.5. Numerical simulation

The numerical solutions for the pulsatile flow in stenosed channel were determined using CFX 16.1 (ANSYS, Inc., USA). Channel modeling was designed by SolidWorks software (Dassault Systèmes SolidWorks Corp., USA) considering circular segment of stenosed part with circular radius of 811.5  $\mu\text{m}$  and central angle of 101.85°. The laminar regime of the momentum equation was applied. The conservation equations for the transient state were solved for the coupling of the velocity and pressure. In this analysis, a no-slip condition was applied to every wall of the channel. The convergence criteria were  $10^{-5}$  for both the momentum and the continuity equations. Through FFT algorithm based on the experimental data, equation for transient mass flow rate was obtained. To minimize the influence of initial flow conditions, all simulations were carried out for three cycles. The inlet channel was extended to 5D length to make fully developed flow. An open condition with a relative pressure of 0 Pa was employed at the outlet of the channel. To describe non-Newtonian behavior for Sample 1 and Sample 2, the Carreau-Yasuda model equation was used by fitting measured viscosity for them. After checking with a preliminary grid dependency test, approximately 6,000,000 nodes were used in the present study.

## 3 Results and discussion

### 3.1 Velocity variation in pulsatile flow

The pulsatile flow was controlled based on the flow rate which is within 0.4 - 3 mL/h in all case. The period of pulsatile flow was 10 s per cycle. The velocity was accelerated as the flow passed through the stenosed channel. Since the velocity profile repetitively varied owing to the pulsatile flow condition, the velocity was expressed depending on the phase ( $\varphi$ ) states. Therefore, the period of one cycle was equal to  $\varphi = 1$ . The flow accelerated from  $\varphi = 0$  to  $\varphi = 0.2$ , and the accelerated flow approached the maximum value at around  $\varphi = 0.2$ . The velocity steeply decreased in the early deceleration phase (from  $\varphi = 0.2$  to  $\varphi = 0.4$ ) and then gradually decreased until  $\varphi = 1.0$ .

### 3.2. Velocity vector fields

The similar velocity distributions were observed in the both cases; the flow acceleration in front of the stenosis, maximum velocity region around the stenotic apex, and flow deceleration in the post-stenosis region. In the case of  $\varphi = 0.2$ , this high velocity region around the stenotic apex (around  $x/D = -1$  to 1) was more skewed toward the stenosed wall ( $r/D = 0$ ) than that in the case of  $\varphi = 0.4$ . At  $\varphi = 0.2$ , the inlet flow state was at the end of acceleration and then reached the maximum velocity. At the same time, it accelerated once again by sudden reduction of diameter, and the direction of the flow was then changed owing to the shape of the stenosis. Therefore, this streamwise flow tended to flow along the center of the longitudinal axis continuously and passed through the channel with high velocity, showing a skewed trend

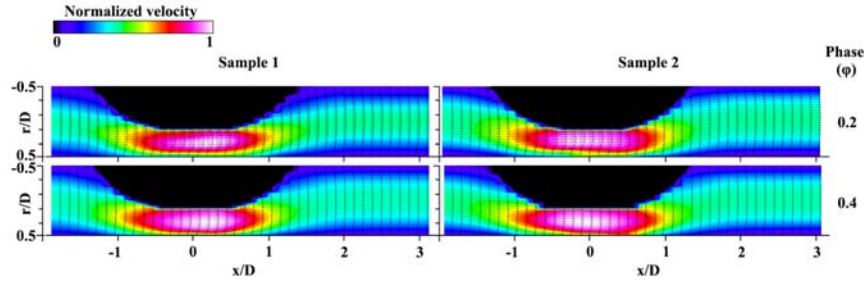


Figure 1: Contoured vector fields representing normalized velocity at  $\varphi = 0.2$  (systolic phase) and  $\varphi = 0.4$  (early diastolic phase) for normal blood and highly viscous blood

to the stenosed wall. The highly accelerated region during deceleration ( $\varphi = 0.4$ ) appeared wider than that at  $\varphi = 0.2$ . Furthermore, the lowest velocity portion in sample 1 and 2 occupied the narrower region near the wall. It implies that the velocity profiles of sample 1 and 2 are blunter. Velocity fields at  $\varphi = 0.2$  from simulation results and it is similar with the trend of experimental results. For sample 1 and 2, the velocity distributions are blunt since velocity region at the center of longitudinal axis has lower value and the lowest velocity region near the wall occupies narrower portion.

### 3.3. WSS distributions

Based on the measured velocity information, the WSR can be roughly estimated by employing the following simplified equation.

$$WSR = \frac{dv}{dr} \approx \frac{v(r_w) - 0}{r_w} \quad (1)$$

where  $v(r_w)$  is the closest velocity data to the wall and  $r_w$  is the relevant distance from the wall in the  $r$ -coordinate. Considering the non-Newtonian feature of the samples, the WSS can be reasonably calculated by multiplying the WSR obtained using Eq. (1) and relevant viscosity at the corresponding WSR [ $\mu$  (WSR)].

$$WSS = \mu(WSR) \cdot WSR \quad (2)$$

To compare the degree of variation among the parameters, each curve was normalized on the basis of their maximum value within the range of  $\varphi = 0.0 - 0.4$ . The non-Newtonian fluids showed dampened descending and ascending slopes for the WSS and a steeper slope for the corresponding WSR. In addition, this trend in **Sample 2** was more intensified than that in **Sample 1**, since the viscosities of these fluids increased with decreased shear rates; further, the degree of increased viscosity was higher in **Sample 2** than in **Sample 1**.

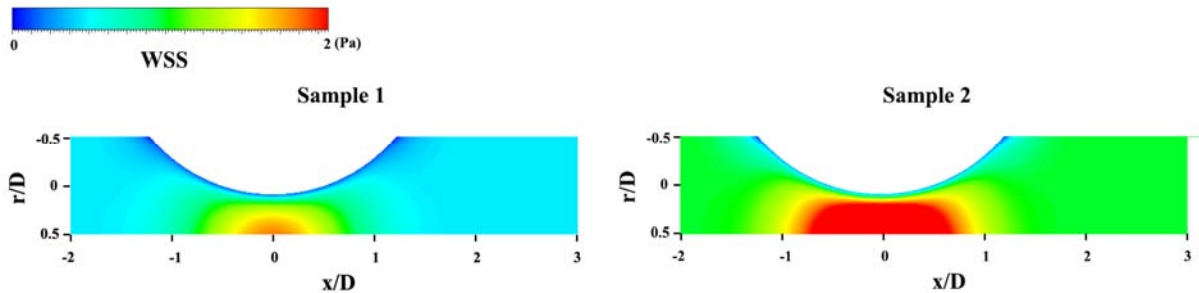


Figure 2: Contoured WSS fields at  $\varphi = 0.2$  (systolic phase) for normal blood and highly viscous blood

In Fig. 2, WSS distributions of samples from the simulation results were represented at 0.2 (systolic phase). In systolic phase, the WSS for the stenosed wall along the flow stream was compared depending on the samples. As the viscosity level of sample increased, the WSS around the stenosis also increased. It reflects similar trends in terms of the absolute magnitudes and the variations of WSS for three fluids, considering the experimental data. The high difference of WSS between upstream and downstream is observed in case of Sample 2. Therefore, the increased viscosity can be considered as the influence factor on the high magnitude and variance of WSS as well as the distinct WSS at the pre-stenosis and the post-stenosis. High WSS magnitude occurred, and variance of WSS through the stenosed structure was apparent in the case of high viscosity fluid (Sample 2). The high magnitude of the WSS gradient contributes to endothelial cell alignment depending on the variation (Dolan et al., 2011). Furthermore, the combined effect between the WSS and WSS gradient is correlated with endothelial cell activation of relevant proteins (Tzima et al., 2005). The responses can result in vascular diseases, such as plaque instability or rupture and tissue layer damage (Dolan et al., 2013).

## 4 Conclusion

Through the PIV measurement, the velocity profiles and WSS variations were estimated around the stenosed microchannel along the phases of pulsatile flow for non-Newtonian fluids. Considering the pulsatile blood flow can contribute to stenosed shapes, the increase in the WSS and the oscillating WSS in highly viscous fluids can damage the blood cells, endothelium, or stenotic lesions. Although this study cannot directly explain the mechanism related to vascular pathology, the lipid accumulation is associated with WSS and flow behavior caused by stenotic structure and pulsatile flow with regard to viscosity variations in blood analog fluids.

## Acknowledgements

This work was supported by Convergence Medical Institute of Technology R&D project (CMIT2019-04), Pusan National University Hospital.

## References

- Anastasiou, AD, Spyrogianni, AS, Koskinas, KC, Giannoglou, GD, and Paras, SV (2012) Experimental investigation of the flow of a blood analogue fluid in a replica of a bifurcated small artery. *Medical engineering & physics* 34:211
- Chien, S (1970) Shear dependence of effective cell volume as a determinant of blood viscosity. *Science* 168:977
- Dolan, JM, Meng, H, Singh, S, Paluch, R, and Kolega, J (2011) High fluid shear stress and spatial shear stress gradients affect endothelial proliferation, survival, and alignment. *Annals of biomedical engineering* 39:1620
- Dolan, JM, Kolega, J, and Meng, H (2013) High wall shear stress and spatial gradients in vascular pathology: A review. *Ann Biomed Eng* 41:1411
- Hong, H, Yeom, E, Ji, HS, Kim, HD, and Kim, KC (2017) Characteristics of pulsatile flows in curved stenosed channels. *PloS one* 12:e0186300
- Jahangiri, M, Haghani, A, Ghaderi, R, and Harat, SMH (2018) Effect of non-newtonian models on blood flow in artery with different consecutive stenosis. *International Journal of Advanced Design & Manufacturing Technology* 11:

- Kwak, BR, Back, M, Bochaton-Piallat, ML, Caligiuri, G, Daemen, MJ, Davies, PF, Hofer, IE, Holvoet, P, Jo, H, Krams, R, Lehoux, S, Monaco, C, Steffens, S, Virmani, R, Weber, C, Wentzel, JJ, and Evans, PC (2014) Biomechanical factors in atherosclerosis: Mechanisms and clinical implications. *Eur Heart J* 35:3013
- Mannino, RG, Myers, DR, Ahn, B, Wang, Y, Margo, R, Gole, H, Lin, AS, Guldberg, RE, Giddens, DP, Timmins, LH, and Lam, WA (2015) "Do-it-yourself in vitro vasculature that recapitulates in vivo geometries for investigating endothelial-blood cell interactions". *Sci Rep* 5:12401
- Molla, MM, and Paul, M (2012) Les of non-newtonian physiological blood flow in a model of arterial stenosis. *Medical engineering and Physics* 34:1079
- Nguyen, TT, Biadillah, Y, Mongrain, R, Brunette, J, Tardif, JC, and Bertrand, OF (2004) A method for matching the refractive index and kinematic viscosity of a blood analog for flow visualization in hydraulic cardiovascular models. *Journal of biomechanical engineering* 126:529
- Toraldo, DM, Peverini, F, De Benedetto, M, and De Nuccio, F (2013) Obstructive sleep apnea syndrome: Blood viscosity, blood coagulation abnormalities, and early atherosclerosis. *Lung* 191:1
- Tzima, E, Irani-Tehrani, M, Kiosses, WB, Dejana, E, Schultz, DA, Engelhardt, B, Cao, G, Delisser, H, and Schwartz, MA (2005) A mechanosensory complex that mediates the endothelial cell response to fluid shear stress. *Nature* 437:426
- Wells, RE, and Merrill, EW (1961) Shear rate dependence of the viscosity of whole blood and plasma. *Science* 133:763
- Yeom, E, Kang, YJ, and Lee, SJ (2014) Changes in velocity profile according to blood viscosity in a microchannel. *Biomicrofluidics* 8:034110
- Yeom, E, Kim, HM, Park, JH, Choi, W, Doh, J, and Lee, SJ (2017) Microfluidic system for monitoring temporal variations of hemorheological properties and platelet adhesion in lps-injected rats. *Scientific reports* 7:1801